Article:
Campisi, S, Motta, D, Barlocco, I et al. (5 more authors) (2022) Furfural Adsorption and Hydrogenation at the Oxide-Metal Interface: Evidence of the Support Influence on the Selectivity of Iridium-Based Catalysts. ChemCatChem, 14 (6). e202101700. ISSN 1867-3880

https://doi.org/10.1002/cctc.202101700

Furfural adsorption and hydrogenation at the oxide–metal interface: evidence of the support influence on the selectivity of iridium-based catalysts

Sebastiano Campisi,*[a] Davide Motta,[b] Ilaria Barlocco,[a] Rebecca Stones,[c] Thomas W. Chamberlain,[c] Arunabhiram Chutia,[d] Nikolaos Dimitratos,[e] and Alberto Villa[a]

[a] Dr. S. Campisi, I. Barlocco, Prof. A. Villa
Dipartimento di Chimica,
Università degli Studi di Milano,
via Golgi 19,
20133 Milano, Italy
E-mail: sebastiano.campisi@unimi.it
[b] Dr. D. Motta
Cardiff Catalysis Institute,
School of Chemistry,
Cardiff University,
Cardiff CF10 3AT, UK
[c] Dr. R. Stones, Prof. T.W. Chamberlain
Institute of Process Research & Development,
School of Chemistry,
University of Leeds,
Woodhouse Lane, Leeds LS2 9JT, UK
[d] Dr. A. Chutia
School of Chemistry,
University of Lincoln,
Lincoln LN6 7TS, UK
[e] Prof. N. Dimitratos
Dipartimento di Chimica Industriale e dei Materiali,
ALMA MATER STUDIORUM Università di Bologna,
Viale Risorgimento 4,
40136 Bologna, Italy

Supporting information for this article is given via a link at the end of the document.

Abstract: Here, tetrakis(hydroxymethyl)phosphonium chloride-protected colloidal iridium nanoparticles were deposited by sol-immobilisation on three different supports (CeO_2, NiO and TiO_2) and were investigated for the liquid-phase direct hydrogenation (H_2 atmosphere) and catalytic transfer hydrogenation - CTH (N_2 atmosphere) of furfural to study the effect of the H donor. The occurrence of strong-metal support interactions in 1 wt% Ir/CeO_2 catalyst, as disclosed by XPS, was revealed to be responsible for the high activity observed in the direct hydrogenation (81% conversion after 6h) and for the unusual selectivity to 2-methylfuran (70%) under CTH conditions. On the other hand, Ir/NiO showed peculiar selectivity to tetrahydrofurfuryl alcohol in both H_2 and N_2 atmospheres (71% and 70%, respectively). The density functional theory calculations further showed that the unique selectivity of Ir/NiO may be ascribed to the adsorption properties of furfural on the support, which activates a dual-site hydrogenation mechanism.

Introduction

It is increasingly recognised that a transition towards greener, more sustainable process development is necessary to move away from oil-dependency and overcome severe environmental and climatic issues associated with the large-scale use of fossil fuels. Exploiting renewable chemical supplies as alternatives to fossil resources to satisfy the increasing energy and chemical demands is an obvious place to start in creating strategic models for sustainable process development. Lignocellulosic biomass is a bio-renewable feedstock which can be processed to produce chemicals, biofuels and energy vectors. Several platform molecules can be derived from raw biomass transformation. Among these, furfural (furan-2-carbaldehyde, FF) is typically sourced by hemicellulose (one of the three main components in lignocellulose) through acid-catalysed dehydration of C5 sugars (e.g. xylose), and it is one of the top 12 value-added products, according to US Department of Energy (DOE) classification [1]. Indeed, thanks to the presence of different functionalities (furan ring and carbonyl group), furfural can undergo several chemical transformations, thus serving as a platform molecule to produce fuel additives, fine chemicals, solvents, plasticizers, and resin precursors. In most cases, the conversion of furfural into chemicals or fuels involves hydrogen transfer processes, specifically hydrogenation and hydrogenolysis reactions, together with ring opening, re-arrangement, de-carbonylation and condensation reactions [2,3]. A plethora of interesting chemical compounds, such as furfuryl alcohol (FA), tetrahydrofurfuryl alcohol (THFA), methylfuran (MF), methyl-tetrahydrofuran (MTHFA) and pentanediols (PDs) can be obtained from the reduction of furfural (Scheme 1 a). From this point of view, catalysts and experimental conditions are the main factors which impose a crucial influence on the selectivity in the

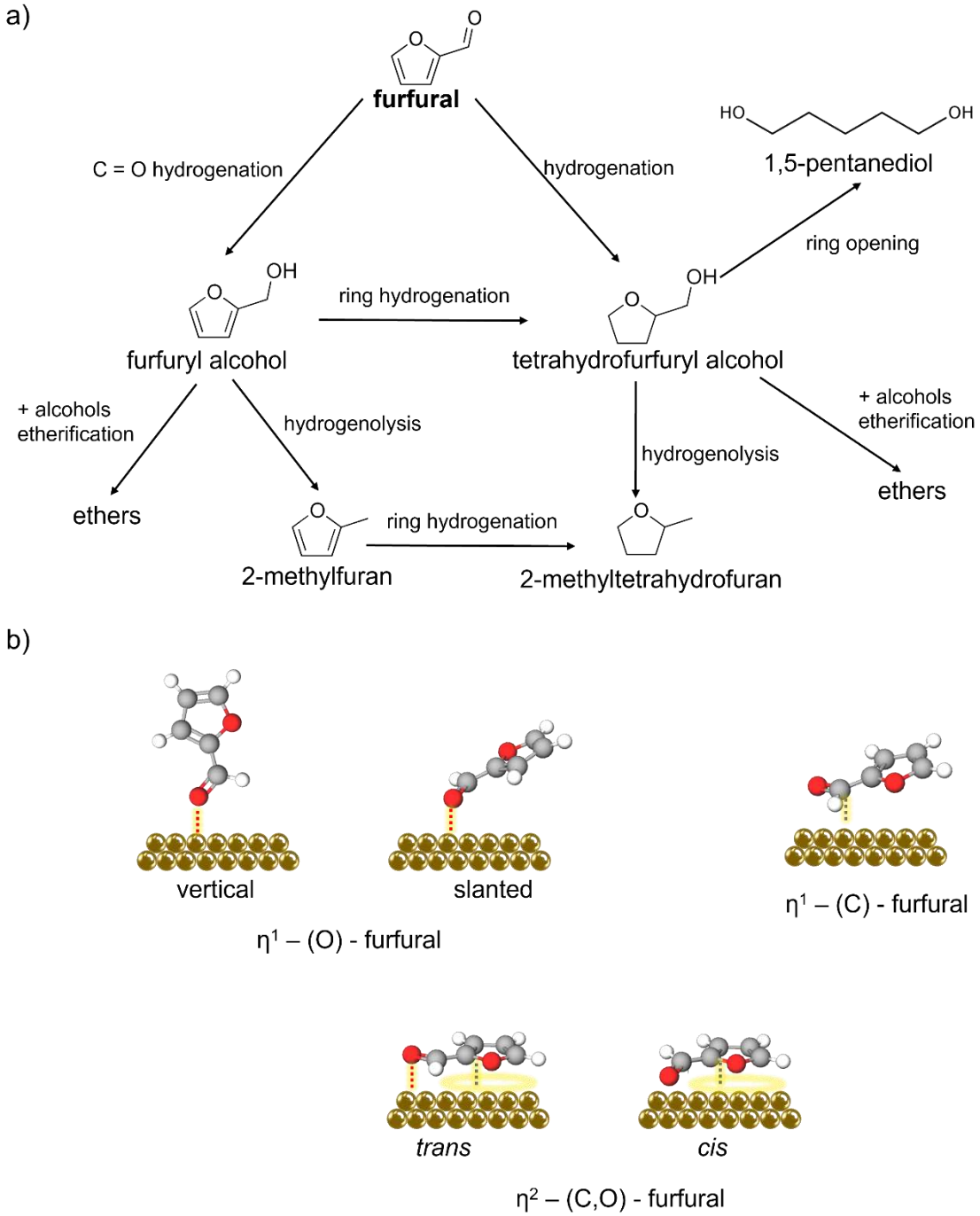

Scheme 1. Furfural reductive conversion. a) Reaction pathway for the hydrogenation of furfural; b) possible adsorption configurations of furfural on metal surfaces.

reductive conversion of furfural [4,5]. Supported noble metal (Pt, Pd, Ru and Ir) as well as transition metal (Cu, Fe, Ni) nanoparticles have been proposed as heterogeneous catalysts for the direct hydrogenation (under H_2 pressure) and the catalytic transfer hydrogenation (using an organic molecule as the hydrogen source) of furfural [6–26]. Depending on the metal nature and structure (distribution of exposed active sites, such as edges, corners, terraces), furfural can adopt different adsorption modes on the active surface [27], which are schematically depicted in Scheme 1 b. Considering that the relative substrate orientation and distance from the metal surface have implications on the catalytic mechanism (e.g. structure of intermediates, stabilization, etc.), controlling the furfural adsorption configuration represents one of the key drivers to direct the reaction pathway and address the selectivity towards target products. In addition, the support, is known to play a fundamental role, for example, strong metal-support interactions (SMSI) can contribute to modulation of the catalytic performances through electronic interactions [28]. Moreover, in some cases, cooperative catalysis between metal nanoparticles and the support surface has been reported for furfural hydrogenation [28–33]. In this regard, we have recently demonstrated that furfural hydrogenation proceeds with enhanced selectivity to tetrahydrofurfuryl alcohol via a dual-site mediated mechanism over a Pd/NiO catalyst: the Pd centre is

responsible for the dissociation of hydrogen, which subsequently spills over onto the NiO support, where furfural is adsorbed and activated [34].

In this work an insight into the role of the support in determining the catalytic performance of supported iridium nanoparticles in furfural hydrogenation is provided. Due to their high activity even under mild conditions, remarkable durability and resistance to leaching, iridium-based catalysts have proven outstanding catalytic performances for a great number of hydrogenation reactions [35–37]. In many cases the catalytic activity and selectivity of Ir-based catalysts are influenced by the environment around the active sites and specifically by the support. The electron-donor/acceptor tendencies of supports can induce charge transfer phenomena and determine the predominant oxidation state of iridium species [38–48]. In particular, electron donor supports, such as ceria and phosphorylated titania, stabilize Ir in the metallic form, which is usually the active species in hydrogenation reactions. Such effects have also been investigated in part in the reductive conversion of furfural, where both monometallic and alloyed Ir-based catalysts have been successfully employed [23,25,30,49,50]. Yu *et al*. have evidenced the remarkable activity of the interface sites of Ir-metal oxide heterostructures, and specifically of Ir/CoO_x, in the reduction of furfural [49]. The beneficial effects deriving from the modulation of metal–support interactions by hydrogen doping into the MoO_3 support for Ir-based catalysts for furfural hydrogenation have been recently highlighted by Xie *et al*. [30]. Herein, preformed, colloidal iridium nanoparticles, synthesized using tetrakis(hydroxymethyl)phosphonium chloride (THPC) as both reducing and protecting agent, were immobilized onto three different metal oxides, namely CeO_2, TiO_2 and NiO. The catalytic performance of the Ir-based catalysts was evaluated in both direct and catalytic transfer hydrogenation of furfural in water. Physico-chemical characterization (transmission electron microscopy (TEM) and X-ray photoelectron spectroscopy (XPS)) together with Density Functional Theory (DFT) simulations were utilised to unravel the interfacial phenomena behind the influence exerted by the supports on the catalytic behaviour of the Ir nanoparticles.

Results and Discussion

The use of tetrakis(hydroxymethyl)phosphonium chloride (THPC) as stabilizer and reductant assured the generation of ultrasmall Ir nanoparticles with narrow particle size distribution (d = 1.94 ± 0.24 nm), as confirmed by TEM analyses (Fig. 1 a).

Besides providing optimal size control, THPC prevented the agglomeration of Ir NPs upon deposition onto the selected supports, in agreement with previous reports from the literature [51,52]. Indeed, the immobilization on CeO_2, TiO_2 and NiO produced a high dispersion of THPC-protected Ir NPs with particle diameters (Fig.1 and Table 1) consistently smaller than the unsupported sample (Fig. S1). Moreover, the immobilization was almost quantitative, with experimental loading values, determined by ICP-MS (Table 1), being close to the nominal value of 1 wt.%).

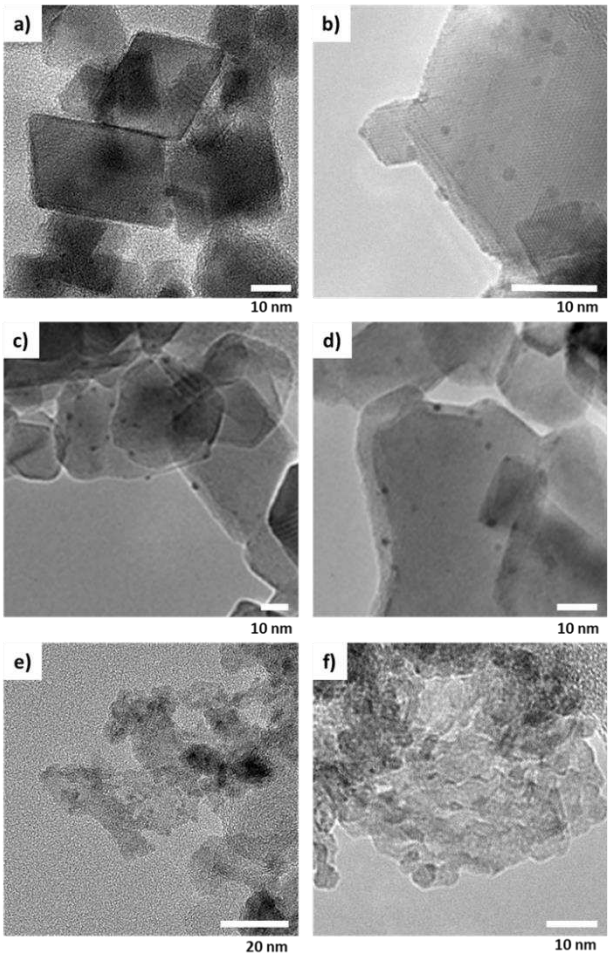

Figure 1. Representative TEM images of a-b) Ir/CeO_2; c-d) Ir/TiO_2 and e-f) Ir/NiO.

Although the three samples possessed similar Ir loading and essentially identical particle size distributions, the analysis of surface composition by X-ray photoelectron spectroscopy (XPS) revealed significant discrepancies in the Ir surface concentration among the samples (Table 1). The highest surface Ir concentration of Ir/NiO might be associated with the enhanced surface area of NiO support (ca. 200 $m^2 g^{-1}$) compared to the other supports (ca. 40-60 $m^2 g^{-1}$). However, it should also be mentioned that the quantification of Ir by XPS in Ir/TiO_2 and Ir/NiO was complicated by overlapping with the photopeaks of Ti 3s and Ni 3s, respectively.

Table 1. Bulk and surface properties of Ir-based catalysts

Catalyst	Ir loading (wt. %)	Ir atomic surface coverage (at. %)	Particle size (nm)
Ir/CeO_2	1.04 ± 0.13	0.86	1.00 ± 0.24
Ir/TiO_2	0.89 ± 0.08	0.39 [a]	1.25 ± 0.21
Ir/NiO	1.0 ± 0.1	1.73 [b]	1.31 ± 0.26

[a] Quantification affected by error due to overlapping with the Ti 3s photopeak
[b] Quantification affected by error due to overlapping with the Ni 3s photopeak.

Table 2. Reaction data for direct hydrogenation of furfural in 2-propanol at 150 °C

Catalyst [a]	Conversion [e]	Selectivity [f]

	k_{app} [b] (min^{-1})	Initial activity tot[c] (h^{-1})	Initial activity surf [d] (h^{-1})	(%)	(%)					
					FA	THFA	2-MF	2-MTHF	Ether	GVL
Ir/CeO_2	$4.6 \cdot 10^{-3}$	190	193	81	73.1	0.3	15.2	2.5	1.8 [g]	2.6
Ir/TiO_2	$1.8 \cdot 10^{-3}$	70	88	45	66.2	0.2	14.1	0.4	0.5 [g]	12.8
Ir/NiO	$4.1 \cdot 10^{-3}$	200	266	75	3.6	72.1	1.3	18.3	2.3 [h]	-

[a] Reaction conditions: Furfural = 0.3 M; FF/metal ratio=500 wt/wt, 150 °C, **5 bar H_2**
[b] Apparent first-order reaction rate constant derived from the slope of the linear plot of ln(1 – *x*) versus time (where *x* is the furfural conversion).
[c] Calculated after 30 min of reaction as $mol_{FF\ converted} \cdot mol_{Ir\ Total}^{-1} \cdot h^{-1}$
[d] Calculated after 30 min of reaction as $mol_{FF\ converted} \cdot mol_{Ir\ Surf}^{-1} \cdot h^{-1}$
[e] Furfural conversion after 6 h
[f] Selectivity at ca. 45% of conversion
[g] Isopropyl furfuryl ether
[h] Isopropyl tetrahydrofurfuryl ether

The catalytic performances of supported Ir catalysts in the direct hydrogenation of furfural were evaluated under batch conditions (T = 150 °C, $p(H_2)$ = 5 bar, with 2-propanol as the solvent) with the aim to probe the effect of the support.

Furfural conversion after 6 h of reaction (Table 2) decreased in the following order: Ir/CeO_2 (81%) > Ir/NiO (75%) >> Ir/TiO_2 (45%). The trend was also confirmed by the computation of the apparent rate constant. Based on previous reports from the literature [28,53], first order kinetics were assumed for the furfural hydrogenation. The assumption was validated by the linear fitting of the plots of $-\ln(1 - X_a)$ versus reaction time (Fig. S2, where X_a represents FF conversion), which is typical of first order reactions. From the slope of the first order fit the values of the apparent rate constants were derived and reported in Table 2. The apparent first-order kinetic constant values reflected the activity order derived from the conversion data: $Ir/CeO_2 \approx Ir/NiO >> Ir/TiO_2$. Interestingly, k_{app} values for Ir/CeO_2 and Ir/NiO are of the same order of magnitude as those reported in the literature for other catalytic systems, which worked under harder experimental conditions, such as Pd/oxides (180 °C, 20 bar H_2) [28] and Co–Cu/SBA-15 (150 °C, 30 bar H_2)[53]. The same ranking was obtained considering initial activity ($mol_{converted} \cdot mol_{Ir,tot}^{-1} \cdot h^{-1}$, Table 2). The activity values of Ir/CeO_2 and Ir/NiO are superior or comparable to those of other promising Ir-based catalysts reported in the literature (e.g. in Table S.2), although a valid comparison is not possible, due to the differences in the adopted experimental conditions. The modest activity of Ir/TiO_2 might be related to the Ir surface concentration, which was markedly lower in Ir/TiO_2 than in the other catalysts. Nevertheless, the Ir surface concentration alone is not sufficient to rationalize the observed activity trend. Indeed, if the activity was determined solely by the number of exposed surface Ir atoms, the normalization of activity values with respect to the amount of surface Ir atoms should produce values (Initial activity surf = $mol_{converted} \cdot mol_{Ir surf}^{-1} \cdot h^{-1}$) similar for the three catalysts. However, initial $activity_{surf}$ values computed by considering the mean particle size derived from TEM, and by assuming hemispherical shaped particles, reflected the same trend observed for k_{app} and initial activity (Table 2), thus confirming that surface Ir exposition cannot be the sole parameter affecting the catalyst activity. On the other hand, although furfural hydrogenation is known to be a structure-sensitive reaction, in our case the very similar particle sizes of Ir-based catalysts, suggest excluding important structural differences and different proportion of surface adsorption sites (terrace sites, edges and corners) among the tested catalysts. Thus, the observed discrepancies in terms of activity seem to be determined mainly by the support nature.

Actually, remarkable differences emerged also in the selectivity (evaluated at a similar furfural conversion (40%)) depending on the support (Table 2). The reaction seems to proceed with a similar reaction pathway over Ir/CeO_2 and Ir/TiO_2, which were able to preferentially hydrogenate furfural to furfuryl alcohol (FA selectivity of 73.1% and 66.2%, respectively), similarly to other metal species (Cu, Co, Ru, Pd, Pt) supported on ceria and titania (Table S.3).

Alongside furfuryl alcohol (FA), which is used primarily as a monomer for resins and solvent, 2-methylfuran (2-MF) was obtained as the main side-product (ca. 15%), deriving from the consecutive hydrogenolysis of FA. Notably, gamma-valerolactone (GVL) was also produced in significant quantities over Ir/TiO_2 (13% selectivity). The formation of GVL from furfural has been proven in the literature to proceed according to a Meerwein Ponndorf Verley (MPV) cascade mechanism [54]. From selectivity versus conversion plots (Fig.S.3) it emerges that etherification is predominant at low conversion values (<20%), while increasing the furfural conversion furfuryl alcohol is favoured. For conversion values higher that 45%, the selectivity to FA slightly decreases and products from consecutive reactions (2-MF) are formed.

Different selectivity was observed over Ir/NiO catalyst, which promoted the total hydrogenation of FF to tetrahydrofurfuryl alcohol (72.1 % selectivity), a widely used low-cost and water miscible solvent. THFA then underwent hydrogenolysis to generate 2-MTHF (18%), a commercially used solvent.

From product distribution plots as a function of reaction time or conversion (Fig. 2 and Fig. S.3) it appears clear that the FF is preferentially hydrogenated to THFA over Ir/NiO at all time points and at each FF conversion value, thus indicating that a different pathway is followed over this catalyst compared to Ir/CeO_2 and Ir/TiO_2. Furthermore, the peculiar behaviour of Ir/NiO is in line with what has been already observed over NiO and Pd/NiO [34].

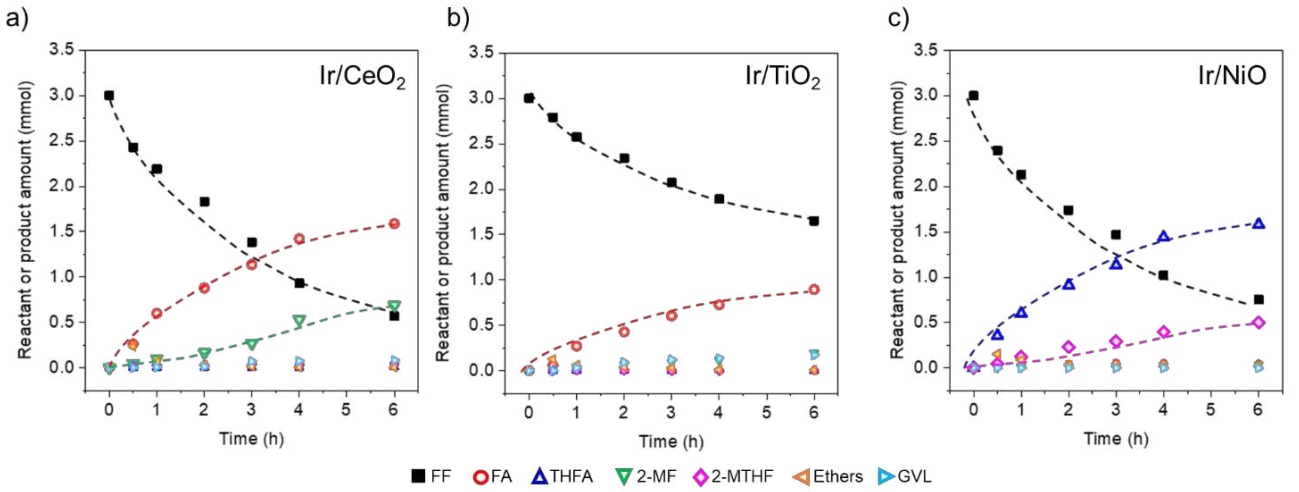

Figure 2. Time-online profiles of furfural and main products over a) Ir/CeO_2, b) Ir/TiO_2 and c) Ir/NiO. Reaction conditions: Furfural = 0.3 M; FF/metal ratio=500 wt/wt, 150 °C, 5 bar H_2.

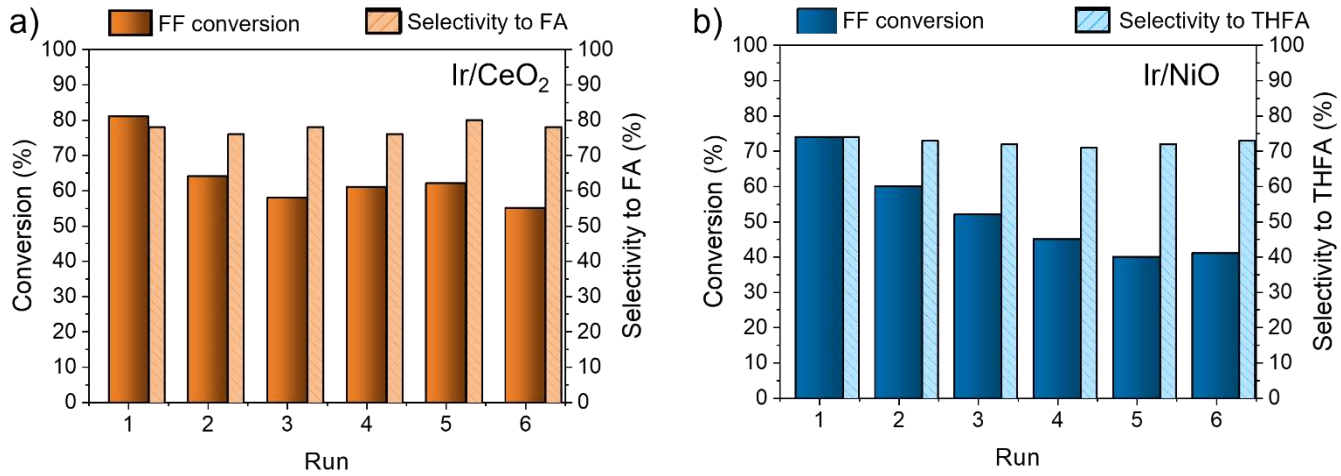

Figure 3. Stability tests using a) Ir/CeO_2 and b) Ir/NiO. Reaction conditions: Furfural = 0.3 M; FF/metal ratio=500 wt/wt, 150 °C, 5 bar H_2.

However, making a fair comparison with literature data (Table S.2) is not trivial, since different operating conditions as well as different catalytic properties (e.g. Ir loading, particle size),

The stability of the two most active catalysts, Ir/CeO_2 and Ir/NiO, was assessed by reusability tests (Fig. 3). An initial decrease from ~80% to ~60% in FF conversion was observed in the case of Ir/CeO_2 between the first and second run, after which no further decrease in activity was detected over 6 runs. Conversely, the catalytic activity of Ir/NiO continuously and gradually declined until reaching a plateau around 40% of conversion (5^{th} and 6^{th} runs). Interestingly, in both catalysts no significant changes were observed in the selectivity over six runs, being FA and THFA the main products of FF hydrogenation on Ir/CeO_2 and Ir/NiO, respectively. According to leaching experiments, the observed loss of activity might be related to a partial Ir dissolution, which was more pronounced in the case of Ir/NiO. On the other hand, the evidence of unaltered selectivity values suggests that no remarkable modification of the morphology, structure and oxidation state of Ir NPs has occurred.

The evidenced differences in terms of activity, selectivity and stability among the three Ir-based catalysts call for a deeper investigation looking into the causes of such catalytic behaviors.

As mentioned above, the discrepancies in activity cannot be ascribed uniquely to the Ir surface concentration. On the other hand, the three catalysts have identical particle sizes (Table 1), thus this descriptor can be also ruled out. The occurrence of metal-support interactions and charge-transfer from the supports to the Ir NPs might be invoked to interpret the different catalytic behaviour of the studied catalysts. High resolution XP spectra in the Ir 4f region were collected to investigate the oxidation state of Ir and disclose eventual electronic metal-support interactions.

High resolution Ir 4f spectra of Ir/CeO_2, Ir/TiO_2 and Ir/NiO are comparatively reported in Fig. 4. In all the spectra Ir 4f signal presented the typical spin-orbit splitting in Ir $4f_{7/2}$ (60.8–62.8 eV) and Ir $4f_{5/2}$ (63.8–65.8 eV) components. Each spin-orbit

component in the spectra of Ir/CeO_2 and Ir/NiO may be further decomposed into two sub-peaks, while in the case of Ir/TiO_2 the complexity of the signal (due to overlapping with Ti 3s photopeaks) did not allow for such distinction. In all cases the theoretical values of area ratio (Ir $4f_{7/2}$:Ir $4f_{5/2}$ = 4:3) and splitting energy ($\Delta \approx 3$ eV) were satisfied.

According to the literature [55], the intense feature centred at 60.9 eV for the Ir $4f_{7/2}$ peak (and 64.0 eV for Ir $4f_{5/2}$) in Ir/NiO could be associated with metallic Ir(0) and accounted for 84.9% of the total area, while the doublet with sub-peaks at 62.7 eV (Ir $4f_{7/2}$) and 65.8 eV (Ir $4f_{5/2}$) is typical of Ir(IV) species, likely partially oxidized IrO_x species (15.1%). These species were also present also in Ir/CeO_2 (sub-peaks at 62.6 and 65.8 eV), which constituted 12.9% of the surface Ir species. The prominent feature in the Ir 4f spectrum of Ir/CeO_2 was characterized by peaks at 61.7 eV (Ir $4f_{7/2}$) and 64.8 eV (Ir $4f_{5/2}$), which were shifted to higher binding energies compared to typical values for Ir(0). Such an up-shift (≈ 0.7-0.8 eV) has been already reported in the literature for small Ir nanoparticles supported on a CeO_2 (111) film and was attributed to charge-transfer phenomena at the metal-oxide interface, which implies reduction of Ce^{4+} cations to Ce^{3+} and the simultaneous insurgence of a partial positive charge (δ+) on the iridium nanoparticles.[56]

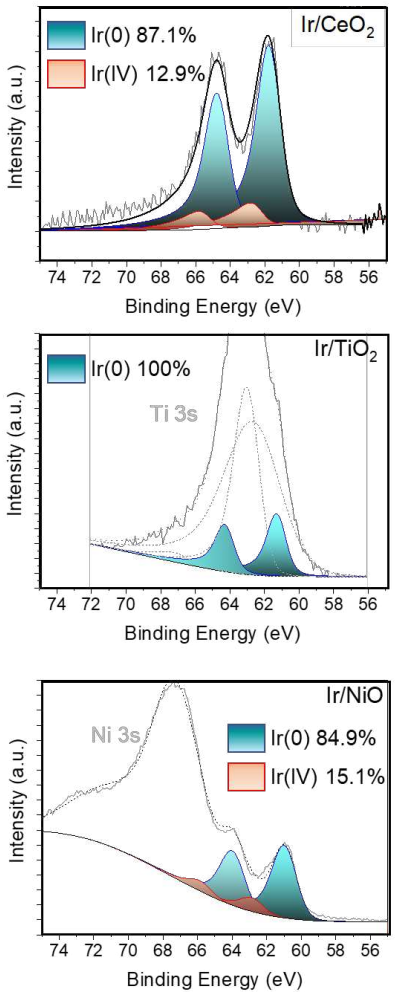

Figure 4. High resolution Ir 4f spectra of a) Ir/CeO_2, b) Ir/TiO_2 and c) Ir/NiO.

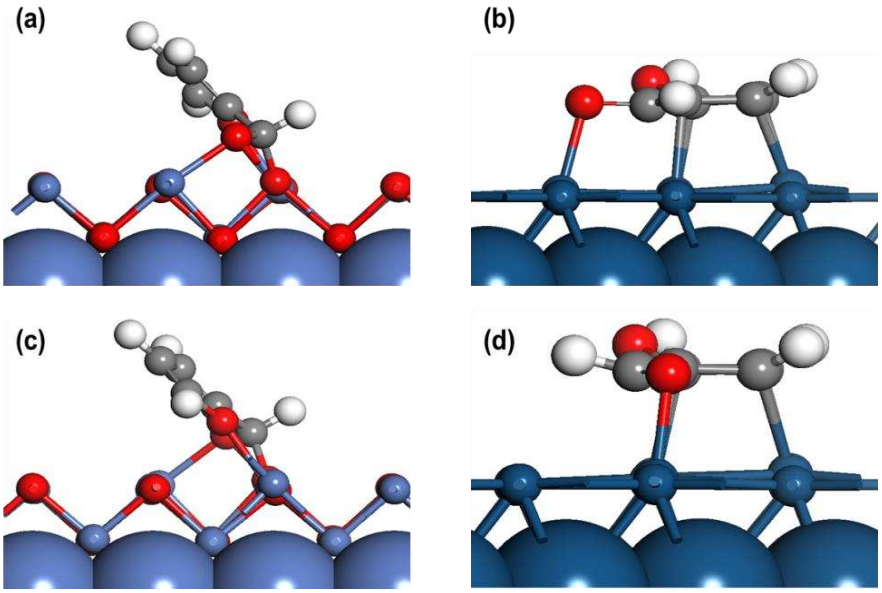

Figure 5. The fully relaxed structures of the cis-furfural molecule on (a) NiO(110) and (b) Ir(111) surfaces and the trans-furfural molecule on (c) NiO(110) and (d) Ir(111) surfaces. For clarity the furfural molecule and the top two layers of the Ni(110) and the Ir(111) surfaces are shown as ball and stick representations and the rest of the models are depicted in the CPK form (carbon is represented in grey, hydrogen in white, oxygen in red, nickel in purple and iridium in blue).

SMSI between Ir NPs and the ceria support have been already demonstrated to have a crucial influence on the catalytic performance in the carbon dioxide reaction [38]. Consequently, in our case also the occurrence of electronic metal-support interactions, which were observed exclusively on Ir/CeO_2, could be responsible for the higher FF conversion observed on this catalyst compared to the other two. Moreover, due to the strong interactions, Ir NPs are firmly anchored on ceria, and this could explain the higher stability of Ir/CeO_2 compared to Ir/NiO in the reusability tests. Indeed, the stable anchorage of Ir NPs onto ceria support prevents Ir leaching, which has been proposed to be the primary cause of deactivation on the studied catalysts.

Concerning the selectivity, the presence of specific SMSI in Ir/CeO_2 cannot justify the detected differences in the resultant product distributions. Indeed, despite the different activity, Ir/CeO_2 and Ir/TiO_2 seemed to promote the same reaction pathway, where FA and MF were the main products, while Ir/NiO stood out for its unique selectivity to THFA.

The reason behind the peculiar selectivity of Ir/NiO could be a result of the unique capacity of the NiO support to adsorb and activate the furfural molecule, as already reported for Pd/NiO catalysts[34].

Actually, catalytic tests carried out on the bare supports (CeO_2, TiO_2 and NiO) demonstrated that only NiO was active in the furfural hydrogenation, while no activity was detected on ceria and titania (Table S.1). Moreover, the reaction proceeded with high selectivity to THFA over NiO as in the case of Ir/NiO. These observations corroborate with the hypothesis of a cooperative mechanism in which both Ir NPs and NiO is active in the Ir/NiO catalyst, similar to Pd/NiO[34].

For further confirmation, the unique effect of NiO support in directing the selectivity was investigated by density functional theory with dispersion corrections. The DFT+D3 calculations showed that the furfural molecule, firstly considered in cis conformation, is more stable on the NiO(110) surface with an adsorption energy of -2.572 eV as compared to the Ir(111) surface (adsorption energy = -2.028 eV). As shown in Figure 5, on the Ni(110) surface the furfural molecule is adsorbed via the O-atoms of the furan ring and the C of the CHO group. On the other hand, on the Ir(111) surface the furfural molecule is adsorbed via the O-atom of the CHO group and C-atoms of the furan ring. We also investigated the effect of the trans-conformations of the furfural molecule (see Scheme 1(b)) on the most stable configurations of the NiO(110) and the Ir(111) surfaces. Our calculations reveal that the adsorption energies of trans-furfural/Ni(110) and trans-furfural/Ir(111) surfaces are -2.445 eV and -2.229 eV respectively, which clearly shows that the trend of higher stability of the furfural molecule on our models of Ni(110) and Ir(111) surfaces does not change. Further to this, as shown in Figure 5 (c and d) the mode of adsorption also remains the same. Previous kinetic studies reported a -0.5 global order (0.5 with respect to furfural and -1 with respect to H_2) for furfural hydrogenation on Ir/TiO_2, calculated on initial rate.[57] A typical single-site Langmuir–Hinshelwood kinetic model (LH) has been invoked[57], involving the dissociative adsorption of hydrogen and the surface reaction between chemisorbed hydrogen and adsorbed furfural on the same site. In our case, the preferential adsorption of furfural on NiO and the relative configuration seem to suggest that a dual-site hydrogenation mechanism is active, as already proposed for Pd/NiO[34]; hydrogen is firstly dissociated on the Ir metal surface, then H_{ads} migrates onto the NiO surface where furfural is adsorbed and then reduced (Scheme 2). The peculiar η^2-(C,O)-furfural adsorption configuration on NiO could promote the complete hydrogenation of furfural, thus being responsible for the unique selectivity to THFA. Conversely, according to literature data[57], a single-site LH mechanism could be proposed for Ir/CeO_2 and Ir/TiO_2: chemisorbed H reacts with furfural molecule adsorbed onto vicinal site at Ir surface. The preferential adsorption of furfural on the Ir surface via the O-atom of the CHO group could in this case justify the high selectivity to FA of Ir/CeO_2 and Ir/TiO_2 catalysts.

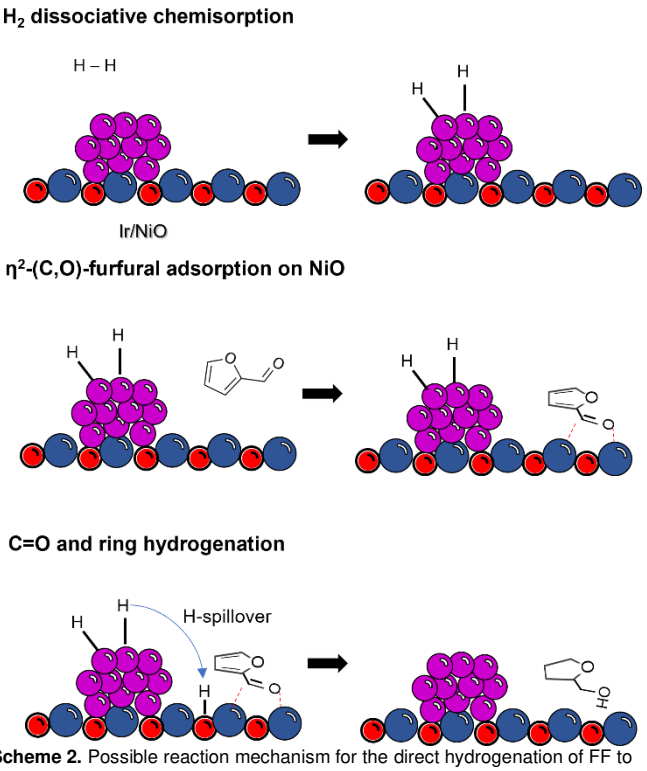

Scheme 2. Possible reaction mechanism for the direct hydrogenation of FF to THFA over Ir/NiO catalyst.

The two most promising catalysts, Ir/CeO_2 and Ir/NiO, were also tested in the catalytic transfer hydrogenation of furfural in 2-propanol as the H-donor. From the results listed in Table 2, a different scenario emerged compared to direct hydrogenation. Indeed, when H_2 is replaced by N_2, the activity trend is reversed, with Ir/NiO (64% conversion after 6 h) more active than Ir/CeO_2 (48% conversion after 6 h). In particular, the activity of Ir/CeO_2 in the catalytic transfer hydrogenation is observe dto be significantly lower than in the direct hydrogenation. This evidence seems to suggest that the interfacial sites, which are supposed to be responsible for the high activity of Ir/CeO_2 in the presence of H_2, are less effective in the catalytic hydrogen transfer. Interestingly, the selectivity of Ir/NiO was the same regardless of whether H_2 or N_2 is present, while, conversely, the selectivity of Ir/CeO_2 changed under CTH conditions.

Table 3. Furfural catalytic transfer hydrogenation in 2-propanol at 150 °C

Catalyst[a]	Conversion[b]	Selectivity[c]

	(%)	(%)					
		FA	THFA	2-MF	2-MTHF	Ether	GVL
Ir/CeO_2	48	16.1	0.5	70.2	2.9	2.4[d]	4.4
Ir/NiO	64	2.0	70.5	0.4	22.8	2.3[e]	-

[a] Reaction conditions: Furfural = 0.3 M; FF/metal ratio=500 wt/wt, 150 °C, **5 bar N_2**
[b] Furfural conversion after 6 h
[c] Selectivity at ca. 50% of conversion
[d] Isopropyl furfuryl ether
[e] Isopropyl tetrahydrofurfuryl ether

Specifically, the main product for long reaction times in this case is 2-MF (70.2%), which is produced by FA hydrogenolysis (while for short reaction times etherification to 2-(isopropoxy)methyl furan is favoured in agreement with the literature, Fig. S4). This is an important result, since there are only a few reported examples of the selective conversion of furfural into 2-methylfuran in liquid phase and under CTH conditions[25,58–60]. Vlachos *et al.* combined isotopic labelling and detailed kinetic studies to demonstrate that a dual active site, tandem mechanism is involved in the catalytic transfer hydrogenation of furfural to 2-methylfuran on a bifunctional $Ru/RuO_x/C$ catalyst. In particular, Lewis acid sites promote the hydrogenation of the aldehydic group of furfural to furfuryl alcohol via an intermolecular hydride transfer, while both metal and Lewis acid sites are required to catalyse the hydrogenolysis of furfuryl alcohol through ring-activation [61]. According to this mechanism and based on the evidence from XPS analysis, the high selectivity to 2-MF observed on Ir/CeO_2 may be justified by the copresence of metal Ir(0) sites together with $Ir^{\delta+}$ centres, which can act as Lewis acid sites (Scheme 3).

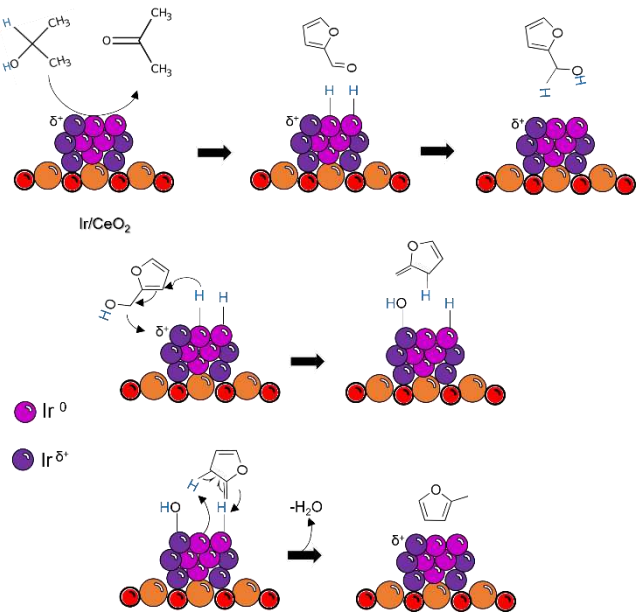

Scheme 3. Possible reaction mechanism for the hydrogenolysis of FF to MF.

Conclusion

In this study we demonstrated that the nature of the support and its interactions with the metal phase as well as with the reagent molecules are critical in the liquid-phase reductive conversion of furfural. When used as the support, CeO_2 triggered strong metal-support interactions with ultrafine, well-dispersed Ir NPs, which influenced both the activity and selectivity of the Ir/CeO_2 catalyst. Specifically, the presence of partially positively charged $Ir^{\delta+}$ sites resulted in an enhancement of conversion in the direct hydrogenation of furfural and conferred Lewis acidity which is beneficial for the preferential production of 2-methylfuran under CTH conditions. On the other hand, NiO is able to strongly adsorb furfural thus directing the selectivity of the Ir/NiO catalyst through a dual site mechanism, which promotes the complete hydrogenation of furfural to tetrahydrofurfuryl alcohol.
These results corroborated the idea that a rational design of heterogeneous catalysts for biomass valorisation cannot disregard a deep understanding and control of the phenomena occurring at the metal-support interface. Only a combined optimization of catalyst design and reaction conditions (solvent, temperature, pressure) could allow biomass-derived chemicals to become competitive with currently widespread petro-based chemicals.

Experimental Section

Materials

All chemicals and gases were obtained from commercial suppliers and employed without any further purification or treatment. Cerium(IV) oxide (CeO_2, SSA: 44 $m^2\ g^{-1}$) from Sigma Aldrich, titanium dioxide (Aeroxide® TiO_2 P25, ≥99.5% purity, SSA: 50 $m^2\ g^{-1}$) from Fisher Scientific. Nickel(II) nitrate hexahydrate ($Ni(NO_3)_2{\cdot}6H_2O$, >99.9% purity) and urea (>99.5% purity) from Sigma Aldrich.
Dihydrogen hexachloroiridiate (H_2IrCl_6, 99% purity) from Alfa-Aesar, sodium hydroxide (NaOH pellets, purity ≥97%) from Fisher Scientific, tetrakis(hydroxymethyl)phosphonium chloride (THPC, purity 99%), sulphuric acid (H_2SO_4, purity 95-98%), furfural (F, purity 99%), 2-propanol (purity 99%), tetrahydrofurfuryl alcohol (purity >99%), 2-methylfuran (purity >99%), tetrahydromethylfuran (purity >99%), isopropyl furfuryl ether (purity >99%), gamma-valerolactone (purity >99%) and n-octanol (purity 99%) were from Sigma-Aldrich.
Pure hydrogen (H_2, 99.99%) and nitrogen (N_2, 99.9999%) gases from Air Liquide were used.

Catalyst preparation

Nickel oxide preparation

Nickel oxide support was prepared by deposition-precipitation starting from nickel(II) nitrate hexahydrate (0.134 M) solution and urea. The desired amount of urea (12:1 mol/mol urea:Ni molar ratio) was solubilized in water, the nickel nitrate solution was then added to reach a final volume of 0.2 L. The solution was maintained at 80 °C under magnetic stirring for 4 h. The suspension was filtered to recover the precipitated nickel hydroxide, $Ni(OH)_2$, from the solution. The solid was thoroughly washed, dried at 100 °C for 2 h and finally calcined at 300 °C for 1 h. The prepared NiO had a surface area value of ca. 210 $m^2\ g^{-1}$.[62]

Supported Ir catalysts preparation by THPC/NaOH colloidal method

Iridium-based catalysts were synthesized using a sol-immobilisation method with tetrakis(hydroxymethyl)phosphonium chloride (THPC), which acts as both reductant and protecting agent, according to the following experimental procedure.

In a 100 mL beaker containing deionised water (50 mL), fresh aqueous solutions of THPC (0.0675 M) and NaOH (0.2 M) were added under stirring to achieve a NaOH/THPC molar ratio of 3:2. After a few minutes, the desired amount of an aqueous solution of the iridium precursor (H_2IrCl_6, 3.25 mg L^{-1}) was introduced (THPC/Ir molar ratio of 4:3) and then left to react under continuous stirring for 30 minutes to achieve the complete reduction of the metal precursor. The reduction reaction progress was monitored by UV/vis spectroscopy. After 25 minutes, when chemical reduction of the metal precursor was complete, the metal nanoparticle solution was immobilised by adding under stirring a weighed mass of support to achieve a 1 wt. % supported catalyst. Depending on the point of zero charge of the support, an acidification step may be required by dropping a concentrated solution of H_2SO_4 (1-1.5 mL). The slurry was left under stirring for 1 h before it was filtered, the catalyst was washed thoroughly with deionised water (1 L) to remove the residues of the reduction reaction and dried at 90 °C overnight under static air. The filtrated solution was collected for analysis with ICP-MS (Agilent 7900 ICP-MS) to verify the actual metal loading.

Catalyst characterization

Tùransmission electron microscopy and energy dispersive X-ray spectroscopy

The samples were dispersed in 2-propanol (10 mL) and treated with sonication for 10 minutes. A few drops of the suspension were deposited on lacey carbon coated copper TEM grids. HRTEM and STEM was performed at 200 kV (Leeds Electron Microscopy and Spectroscopy Centre, LEMAS). NP sizing was performed by measuring a statistically valid number of individual NPs (~100 NPs per sample) using the TEM images. EDX mapping was performed in STEM mode.

X-ray photoelectron spectroscopy

A Thermo Scientific K-alpha+ spectrometer was used to perform X-ray photoelectron spectroscopy (XPS) analyses. The spectrometer uses a monochromatic Al X-ray source operating at 72 W (6 mA x 12 kV). The signal was averaged on an oval-shaped area of approximately 600 x 400 microns. Data was recorded using pass energies of 150 eV for survey scans and 40 eV for high-resolution scans with a 1 eV and 0.1 eV step respectively. Charges on the samples were neutralised using a combination of low energy electrons and argon ions (less than 1 eV) in order to have a C 1s binding energy for adventitious carbon of 284.8 eV. The experimental spectra were fitted after subtraction of Shirley or U2 Tougaard background using CasaXPS (v2.3.17 PR1.1) and Scofield sensitivity factors with an energy exponent of -0.6.

Computational details.

In this study the Vienna Ab initio Simulation Package (VASP) was used to perform all the spin-polarized periodic density functional theory-based quantum chemical calculations.[63,64] The projector augmented wave (PAW) method was used, and the plane wave basis set was expanded using an energy cut off value of 550 eV, which provided the bulk energies convergence to within 10^{-5} eV.[65] For the structural optimization a convergence criterion of 0.01 eV $Å^{-1}$ was selected, and a k-point grid of 3 × 3 × 1 was used for all slab calculations. The Perdew−Burke−Ernzerhof (PBE) version of the generalized gradient approximation (GGA) was used for implementing geometry optimizations and the total energy calculations.[66] To include the dispersive effects, which may play a crucial role in the interaction between the furfural molecule and the surfaces under consideration, the Grimme's dispersion correction as implemented in VASP (DFT+D3) was used.[67] The Ir(111) and NiO(110) were modelled by a 4 × 4 cell with five atomic layers. Of the five atomic layers, the bottom three layers were fixed to simulate the bulk of the material; in the direction perpendicular to the surface, we used a vacuum gap of ~15 Å, which is sufficient to eliminate slab−slab interactions. These slabs were obtained from the theoretically determined lattice constant of 3.843 Å (experimental = 3.839 Å) and 4.192 Å (experimental = 4.168 Å) respectively for the bulk Ir and NiO structures. In this study, the adsorption of the furfural molecule was allowed on only one of the two exposed surfaces and the spurious dipole moment due to the adsorbed species was considered by using the methods implemented in VASP according to the procedures of Neugebauer *et al*. [68,69]. For the calculations on the interaction of furfural on the NiO(110) surfaces we used DFT+U. Previous studies have shown that a U value of 5.77 eV, obtained by using linear response methods, for the d orbital of Ni is suitable.[70]

Catalytic tests

Furfural (FF) hydrogenation was performed at 150°C, using a stainless-steel reactor (30 mL capacity), equipped with heater, mechanical stirrer, gas supply system and thermometer. Furfural solution (15 mL; 0.3 M in 2-propanol) was added into the reactor and the desired amount of catalyst (FF/metal ratio = 500 mol/mol) was suspended in the solution. The pressure of the hydrogen was 5 bar. When catalyst performances in the catalytic transfer hydrogenation (CTH) were tested, experiments were carried out in the same apparatus and under the same experimental conditions (T = 150°C, 15 mL of 0.3 M furfural solution in 2-propanol, FF/metal ratio = 500 mol/mol), except for the pressurized atmosphere, which in CTH tests was constituted by 5 bar of dinitrogen.

The mixture was heated to the reaction temperature, 150°C, and mechanically stirred (1250 rpm). At the end of the reaction, the autoclave was cooled down. Samples were removed periodically (0.2 mL) and HP 7820A gas chromatograph equipped with a capillary column HP-5 30 m x 0.32 mm, 0.25 µm Film from Agilent Technologies. The identification of products was performed using a Thermo Scientific Trace ISQ QD Single Quadrupole GC-MS equipped with a capillary column HP-5 30 m x 0.32 mm, 0.25 µm Film from Agilent Technologies. Authentic samples were also analyzed to determine separation times. Quantitative analysis with external standard method (n-octanol) was used. Initial activity and turn-over frequency were computed at reaction time of 0.5 h and expressed as $mol_{converted} \cdot mol_{Ir,tot}^{-1} \cdot h^{-1}$ and $mol_{converted} \cdot mol_{Ir,surf}^{-1} \cdot h^{-1}$, respectively.

According to Ref., the mols of Ir atoms exposed at the surface and available for reaction ($mol_{Ir,surf}$) was considering the loading of Ir on the samples and the average particle radius (r), determined by TEM, while assuming hemispherical Ir particle shape. The Ir volume (V_{Ir}) per catalyst unit gram was determined from the Ir density ($\rho_{Ir} = 2.256 \times 10^{-23}$ $g_{Ir}/Å^3$) and the Ir weight fraction (w_{Ir}):

$$V_{Ir} = w_{Ir} / \rho_{Ir}$$

Then, the moles of surface Ir per catalyst unit gram were computed using the cross-sectional area of atomic Ir (A_{Ir}; 8.621 Å^2)

$$mol_{Ir,surf} = m \cdot [A_{NP} \cdot (V_{Ir} / V_{NP}) / (A_{Ir} \cdot N_A)]$$

where N_A is the Avogadro number, m is the mass of catalyst and A_{NP} and V_{NP} are the area and volume of one Ir particle of the sample (considering average particle size).

Acknowledgements

AC acknowledges the use of the Cirrus UK National Tier-2 HPC Service at EPCC (http://www.cirrus.ac.uk) funded by the University of Edinburgh and EPSRC (EP/P020267/1) and the use of ARCHER-2 UK National Supercomputing Service (http://www.archer-2.ac.uk) via our membership of the UK's HEC Materials Chemistry Consortium, which is funded by EPSRC (EP/R029431).

Keywords: biomass • heterogenous catalysis • metal-support interactions • spillover • supported catalysts

[1] Y. Zhao, K. Lu, H. Xu, L. Zhu, S. Wang, *Renew. Sustain. Energy Rev.* **2021**, *139*, 110706.
[2] P. Khemthong, C. Yimsukanan, T. Narkkun, A. Srifa, T. Witoon, S. Pongchaiphol, S. Kiatphuengporn, K. Faungnawakij, *Biomass and Bioenergy* **2021**, *148*, 106033.
[3] C. Xu, E. Paone, D. Rodríguez-Padrón, R. Luque, F. Mauriello, *Chem. Soc. Rev.* **2020**, *49*, 4273–4306.
[4] S. Chen, R. Wojcieszak, F. Dumeignil, E. Marceau, S. Royer, *Chem. Rev.* **2018**, *118*, 11023–11117.
[5] H. Xia, C. Chen, P. Liu, M. Zhou, J. Jiang, *Sustain. Energy Fuels* **2020**, *4*, 5709–5720.
[6] R. Zhang, Y. Li, T. Zhen, *RSC Adv.* **2014**, *4*, 52130–52139.
[7] J. A. McCaulley, *Phys. Rev. B* **1993**, *47*, 4873–4879.
[8] R. Insyani, A. F. Barus, R. Gunawan, J. Park, G. T. Jaya, H. S. Cahyadi, M. G. Sibi, S. K. Kwak, D. Verma, J. Kim, *Appl. Catal. B Environ.* **2021**, *291*, 120120.
[9] A. H. Valekar, M. Lee, J. W. Yoon, J. Kwak, D. Y. Hong, K. R. Oh, G. Y. Cha, Y. U. Kwon, J. Jung, J. S. Chang, Y. K. Hwang, *ACS Catal.* **2020**, *10*, 3720–3732.
[10] F. Tang, L. Wang, M. Dessie Walle, A. Mustapha, Y. N. Liu, *J. Catal.* **2020**, *383*, 172–180.
[11] Y. Wang, P. Prinsen, K. S. Triantafyllidis, S. A. Karakoulia, P. N. Trikalitis, A. Yepez, C. Len, R. Luque, *ACS Sustain. Chem. Eng.* **2018**, *6*, 9831–9844.
[12] P. Hou, M. Ma, P. Zhang, J. Cao, H. Liu, X. Xu, H. Yue, G. Tian, S. Feng, *New J. Chem.* **2021**, *45*, 2715–2722.
[13] W. Liu, Y. Yang, L. Chen, E. Xu, J. Xu, S. Hong, X. Zhang, M. Wei, *Appl. Catal. B Environ.* **2021**, *282*, 119569.
[14] Y. Fan, C. Zhuang, S. Li, Y. Wang, X. Zou, X. Liu, W. Huang, G. Zhu, *J. Mater. Chem. A* **2021**, *9*, 1110–1118.
[15] J. Zhang, D. Wu, *Mater. Chem. Phys.* **2021**, *260*, 124152.
[16] Y. Tang, M. Qiu, J. Yang, F. Shen, X. Wang, X. Qi, *Green Chem.* **2021**, *23*, 1861–1870.
[17] G. F. Tierney, S. Alijani, M. Panchal, D. Decarolis, M. B. de Gutierrez, K. M. H. Mohammed, J. Callison, E. K. Gibson, P. B. J. Thompson, P. Collier, N. Dimitratos, E. C. Corbos, F. Pelletier, A. Villa, P. P. Wells, *ChemCatChem* **2021**, *n/a*, DOI https://doi.org/10.1002/cctc.202101036.
[18] A. Shivhare, A. Kumar, R. Srivastava, *ChemCatChem* **2021**, *13*, 59–80.
[19] R. Weng, X. Lu, N. Ji, A. Fukuoka, A. Shrotri, X. Li, R. Zhang, M. Zhang, J. Xiong, Z. Yu, *Catal. Sci. Technol.* **2021**.
[20] Y. Long, S. Song, J. Li, L. Wu, Q. Wang, Y. Liu, R. Jin, H. Zhang, *ACS Catal.* **2018**, *8*, 8506–8512.
[21] X. Gao, S. Tian, Y. Jin, X. Wan, C. Zhou, R. Chen, Y. Dai, Y. Yang, *ACS Sustain. Chem. Eng.* **2020**, *8*, 12722–12730.
[22] M. J. Taylor, L. J. Durndell, M. A. Isaacs, C. M. A. Parlett, K. Wilson, A. F. Lee, G. Kyriakou, *Appl. Catal. B Environ.* **2016**, *180*, 580–585.
[23] N. K. Oklu, B. C. E. Makhubela, *New J. Chem.* **2020**, *44*, 9382–9390.
[24] T. Fovanna, S. Campisi, A. Villa, A. Kambolis, G. Peng, D. Rentsch, O. Kröcher, M. Nachtegaal, D. Ferri, *RSC Adv.* **2020**, *10*, 11507–11516.
[25] N. S. Date, A. M. Hengne, K. W. Huang, R. C. Chikate, C. V. Rode, *Green Chem.* **2018**, *20*, 2027–2037.
[26] Y. Wang, D. Zhao, D. Rodríguez-Padrón, C. Len, *Catalysts* **2019**, *9*, DOI 10.3390/catal9100796.
[27] Z. Yu, X. Lu, X. Wang, J. Xiong, X. Li, R. Zhang, N. Ji, *ChemSusChem* **2020**, *13*, 5185–5198.
[28] H. Lee, C. Nguyen-Huy, E. Jeong Jang, J. Lee, E. Yang, M. S. Lee, J. H. Kwak, K. An, *Catal. Today* **2020**, 0–1.
[29] G. Gao, Y. Shao, Y. Gao, T. Wei, G. Gao, S. Zhang, Y. Wang, Q. Chen, X. Hu, *Catal. Sci. Technol.* **2021**, *11*, 575–593.
[30] L. Xie, T. Chen, H. C. Chan, Y. Shu, Q. Gao, *Chem. - An Asian J.* **2018**, *13*, 641–647.
[31] Z. Zhu, L. Yang, C. Ke, G. Fan, L. Yang, F. Li, *Dalt. Trans.* **2021**, *50*, 2616–2626.
[32] M. J. Gilkey, P. Panagiotopoulou, A. V. Mironenko, G. R. Jenness, D. G. Vlachos, B. Xu, *ACS Catal.* **2015**, *5*, 3988–3994.
[33] M. Y. Byun, D. W. Park, M. S. Lee, *Catalysts* **2020**, *10*, DOI 10.3390/catal10080837.
[34] S. Campisi, C. E. Chan-Thaw, L. E. Chinchilla, A. Chutia, G. A. Botton, K. M. H. Mohammed, N. Dimitratos, P. P. Wells, A. Villa, *ACS Catal.* **2020**, *10*, 5483–5492.
[35] A. S. Rocha, G. C. Costa, L. R. R. de Araujo, W. A. Misael, R. R. Oliveira, A. B. Rocha, *Catal. Letters* **2019**, DOI 10.1007/s10562-019-03056-3.
[36] L. M. Martínez-Prieto, I. Cano, P. W. N. M. van Leeuwen, in (Eds.: L.A. Oro, C. Claver), Springer International Publishing, Cham, **2020**, pp. 397–454.
[37] L. Landenna, A. Villa, R. Zanella, C. Evangelisti, L. Prati, *Cuihua Xuebao/Chinese J. Catal.* **2016**, *37*, 1771–1775.
[38] S. Li, Y. Xu, Y. Chen, W. Li, L. Lin, M. Li, Y. Deng, X. Wang, B. Ge, C. Yang, S. Yao, J. Xie, Y. Li, X. Liu, D. Ma, *Angew. Chemie* **2017**, *129*, 10901–10905.
[39] X. Du, Y. Liu, J. Wang, Y. Cao, K. Fan, *Cuihua Xuebao/Chinese J. Catal.* **2013**, *34*, 993–1001.
[40] M. Babucci, C. Y. Fang, J. E. Perez-Aguilar, A. S. Hoffman, A. Boubnov, E. Guan, S. R. Bare, B. C. Gates, A. Uzun, *Chem. Sci.* **2019**, *10*, 2623–2632.
[41] L. Moriau, M. Bele, Ž. Marinko, F. Ruiz-Zepeda, G. Koderman Podboršek, M. Šala, A. K. Šurca, J. Kovač, I. Arčon, P. Jovanovič, N. Hodnik, L. Suhadolnik, *ACS Catal.* **2021**, *11*, 670–681.
[42] L. Liu, T. Asano, Y. Nakagawa, M. Tamura, K. Okumura, K. Tomishige, *ACS Catal.* **2019**, 10913–10930.
[43] G. Y. Fan, L. Zhang, H. Y. Fu, M. L. Yuan, R. X. Li, H. Chen, X. J. Li, *Catal. Commun.* **2010**, *11*, 451–455.
[44] H. Yu, K. Wada, T. Fukutake, Q. Feng, S. Uemura, K. Isoda, T. Hirai, S. Iwamoto, *Catal. Today* **2020**, DOI 10.1016/j.cattod.2020.02.014.
[45] C. Hammond, M. T. Schümperli, S. Conrad, I. Hermans, *ChemCatChem* **2013**, *5*, 2983–2990.
[46] S. He, L. Xie, M. Che, H. C. Chan, L. Yang, Z. Shi, Y. Tang, Q. Gao, *J. Mol. Catal. A Chem.* **2016**, *425*, 248–254.
[47] K. Wada, H. Yu, Q. Feng, *Chinese Chem. Lett.* **2020**, *31*, 605–608.
[48] M. Babucci, A. S. Hoffman, L. M. Debefve, S. F. Kurtoglu, S. R. Bare, B. C. Gates, A. Uzun, *J. Catal.* **2020**, *387*, 186–195.
[49] H. Yu, J. Zhao, C. Wu, B. Yan, S. Zhao, H. Yin, S. Zhou, *Langmuir* **2021**, *37*, 1894–1901.
[50] Y. Nakagawa, K. Takada, M. Tamura, K. Tomishige, *ACS Catal.* **2014**, *4*, 2718–2726.

[51] J. L. Hueso, V. Sebastián, Á. Mayoral, L. Usón, M. Arruebo, J. Santamaría, *RSC Adv.* **2013**, *3*, 10427–10433.
[52] M. Signoretto, F. Menegazzo, A. Di Michele, E. Fioriniello, *Catalysts* **2016**, *6*, DOI 10.3390/catal6060087.
[53] S. Srivastava, N. Solanki, P. Mohanty, K. A. Shah, J. K. Parikh, A. K. Dalai, *Catal. Letters* **2015**, *145*, 816–823.
[54] J. Iglesias, J. A. Melero, G. Morales, M. Paniagua, B. Hernández, A. Osatiashtiani, A. F. Lee, K. Wilson, *Catal. Sci. Technol.* **2018**, *8*, 4485–4493.
[55] D. Motta, I. Barlocco, S. Bellomi, A. Villa, N. Dimitratos, *Nanomaterials* **2021**, *11*, 1–15.
[56] Y. Lykhach, J. Kubát, A. Neitzel, N. Tsud, M. Vorokhta, T. Skála, F. Dvořák, Y. Kosto, K. C. Prince, V. Matolín, V. Johánek, J. Mysliveček, J. Libuda, *J. Chem. Phys.* **2019**, *151*, DOI 10.1063/1.5126031.
[57] H. Rojas, J. J. Martínez, P. Reyes, *DYNA* **2010**, *77*, 151–159.
[58] P. Panagiotopoulou, D. G. Vlachos, *Appl. Catal. A Gen.* **2014**, *480*, 17–24.
[59] H. Niu, J. Luo, C. Li, B. Wang, C. Liang, *Ind. Eng. Chem. Res.* **2019**, *58*, 6298–6308.
[60] J. Chuseang, R. Nakwachara, M. Kalong, S. Ratchahat, W. Koo-amornpattana, W. Klysubun, P. Khemthong, K. Faungnawakij, S. Assabumrungrat, V. Itthibenchapong, A. Srifa, *Sustain. Energy Fuels* **2021**, *5*, 1379–1393.
[61] M. J. Gilkey, P. Panagiotopoulou, A. V. Mironenko, G. R. Jenness, D. G. Vlachos, B. Xu, *ACS Catal.* **2015**, *5*, 3988–3994.
[62] A. Villa, C. E. Chan-Thaw, G. M. Veith, K. L. More, D. Ferri, L. Prati, *ChemCatChem* **2011**, *3*, 1612–1618.
[63] G. Kresse, J. Furthmüller, *Phys. Rev. B - Condens. Matter Mater. Phys.* **1996**, *54*, 11169–11186.
[64] G. Kresse, J. Hafner, *Phys. Rev. B* **1993**, *47*, 558–561.
[65] P. E. Blöchl, *Phys. Rev. B* **1994**, *50*, 17953–17979.
[66] J. P. Perdew, K. Burke, M. Ernzerhof, *Phys. Rev. Lett.* **1996**, *77*, 3865–3868.
[67] S. Grimme, J. Antony, S. Ehrlich, H. Krieg, *J. Chem. Phys.* **2010**, *132*, 154104.
[68] J. Neugebauer, M. Scheffler, *Phys. Rev. B* **1992**, *46*, 16067–16080.
[69] L. Bengtsson, *Phys. Rev. B - Condens. Matter Mater. Phys.* **1999**, *59*, 12301–12304.
[70] B. Himmetoglu, A. Floris, S. De Gironcoli, M. Cococcioni, *Int. J. Quantum Chem.* **2014**, *114*, 14–49.

Entry for the Table of Contents

Table of Contents

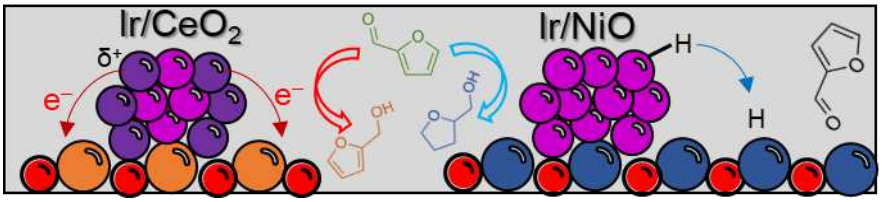

The catalytic behaviour of Ir nanoparticles in furfural hydrogenation is sensitive to the nature of metal-support interphase. Metal-support interactions in Ir/CeO_2 catalyst trigger charge transfer phenomena which enhance the activity and selectivity. A dual-site mechanism is responsible for the unique selectivity of Ir/NiO: furfural is preferentially adsorbed on NiO and therein reduced by hydrogen migrating from Ir surface to the support.